DESIGN OF A UHBR THROUGH FLOW NACELLE FOR HIGH SPEED STALL WIND TUNNEL INVESTIGATIONS

S. Spinner*, R. Rudnik*

* DLR, Institute of Aerodynamics and Flow Technologies, Braunschweig, Germany

Abstract

The design of a new through flow nacelle for the Airbus XRF1 wind tunnel model is presented. The nacelle is representative of a modern UHBR turbofan engine for long range transport aircraft and was especially designed to investigate the interaction of buffet phenomena on the wing lower side, pylon and nacelle within the research unit FOR 2895. During the design process the performance of the through flow nacelle was evaluated by performing RANS simulations with the DLR TAU code using Spalart-Allmaras as well as Reynolds-Stress turbulence models. For the initial nacelle design simulations of the isolated nacelle were performed. Having obtained an initial nacelle shape, it was integrated in the XRF1 CAD model. A pylon geometry was designed and a baseline nacelle position and orientation was defined. The numerical simulations proved the configuration with nacelle and pylon shows adequate performance under cruise conditions without exhibiting unusual adverse effects on the aircraft. As intended, significant shock induced separations were observed on the wing lower side inboard of the nacelle for high speed off-design conditions with negative angles of attack allowing the investigation of buffet phenomena. The numerical results were also used to identify suitable locations for the pressure instrumentation on nacelle and pylon for the wind tunnel test at ETW.

Keywords

Aerodynamic Design; Through Flow Nacelle; Buffet

1. INTRODUCTION

A steady trend towards larger engines with higher bypass ratios can be observed in the aircraft propulsion industry. High bypass ratio engines allow an improved propulsive efficiency by increasing the mass flow rate through the propulsor while the jet velocity is reduced. Nevertheless, care must be taken during the integration process to ensure that the gains in engine efficiency are not outweighed by installation penalties. This requires a close coupling of the engine to the wing in order to provide the necessary ground clearance without extending the landing gear [1] while minimizing interference drag [2].

The integration of a nacelle to a wing comes along with certain aerodynamic installation effects as described in [3]. The flow is straightened by the nacelle reducing the effective angle of attack resulting in an upstream shift of the shock position on the upper wing surface. On the lower surface a virtual half open channel is formed by the engine, pylon, wing lower surface and the fuselage resulting in additional flow acceleration. These effects are even more prominent when the bypass ratio of the engine is increased.

While the above mentioned integration effects are well understood for cruise conditions, there is a demand for research at the border of the flight envelope. The DFG (Deutsche Forschungsgemeinschaft) funded research unit FOR 2895 is dedicated, among other things, to extend the knowledge on high speed stall effects on the wing lower side induced by the installation of a UHBR nacelle. Hybrid RANS/LES methods are to be used to investigate these phenomena allowing the analysis of shock induced separation and buffet with an appropriate level of fidelity that is not possible given by conventional RANS or URANS approaches. However, these hybrid methods require highly accurate reference data for validation purposes. Therefore, wind tunnel experiments funded by the HGF (Helmholtz-Gemeinschaft Deutscher Forschungszentren) in the ETW (European Transonic Wind Tunnel) are performed to characterize the flow field using advanced measurement techniques like Particle Image Velocimetry and Pressure Sensitive Paint. The XRF1 serves as an aircraft configuration. An existing wind tunnel model is provided by Airbus for these investigations. Since only a VHBR through flow nacelle (TFN) without any instrumentation was available for the XRF1 wind tunnel model, a new nacelle had to be designed in order to provide the nacelle and pylon instrumentation required for the validation studies in the FOR 2895. Given the need to build a new TFN, it had been decided to address expected future bypass ratios by selecting a UHBR engine as a target configuration.

The design of the new TFN pursued a twofold objective. On the one hand the nacelle should show representative performance under cruise conditions

to keep the link towards industrial application. On the other hand, buffet phenomena on the wing lower side, pylon and nacelle should be triggered under off-design conditions in order to meet the focus of the FOR2895. Furthermore manufacturing constraints and instrumentation routing for the wind tunnel model had to be considered.

2. METHODOLOGY

The CAD package Catia V5 was used to generate parametric geometries of nacelle and pylon and to integrate them into the XRF1 wind tunnel CAD model. Unstructured meshes were created using the CENTAUR meshing tool with a focus on a fine boundary layer resolution as well as a fine resolution of junctions e.g. between pylon and wing. For investigations of the isolated nacelle, a total number 12.8 million points were used in the mesh. For the nacelle integration studies an aircraft half model with installed TFN was investigated on meshes with a size of roughly 40 million points. Special surface and volume refinement of the mesh was applied to the inboard area on the wing lower side to be able to accurately resolve the transonic phenomena.
Steady RANS simulations of the isolated nacelle were performed with the DLR TAU Code [4] using the negative Spalart-Allmaras turbulence model [5] along with the SARC vortical flow correction model [6] and the QCR extension. Studies on the integrated TFN were done by performing RANS simulations using the SSG/LRR-lnω Reynolds stress model [7] with the use of Menter-BSL-lnω for the RSM length scale equation. A switch to a more sophisticated turbulence model for the integration studies was deemed necessary to allow for a more accurate simulation of corner flow and shock boundary layer interaction phenomena expected for this configuration. For the design and integration phase the assumption was made that strong shock induced separations can be used as an indicator for occuring buffet phenomena.

3. ISOLATED NACELLE DESIGN

The isolated nacelle design focused on adequate performance of the nacelle under cruise conditions. The flow direction was set to the direction of the engine axis (axial inflow).

3.1. Initial Sizing

The initial sizing is based on certain estimates. A consistent design of a UHBR engine was not considered necessary as only the outer contours are required for the targeted investigation of engine/airframe interference effects. Moreover, a through flow nacelle can only mimic displacement effects of the engine, while inlet and jet effects cannot be simulated and have to be neglected, anyway.
The TFN was targeted to be representative of a modern UHBR turbofan engine for a long range transport aircraft with a bypass-ratio of about 15. In order to have a first estimate for the outer dimensions, the existing XRF1 TFN was used as a starting point. By using the area ratio the fan area was scaled up to adjust a higher BPR. A reference area for the core streamtube in the fan plane was estimated. In first approximation it was assumed that the core streamtube area stays constant with increasing BPR. The fan area for the UHBR nacelle was estimated with 8m^2 resulting in a BPR of 16.5 and a fan diameter of 3.192m on the real scale aircraft corresponding to 86.3mm on the wind tunnel model.
The overall length of the outer nacelle for the UHBR TFN was kept similar to the length of the Airbus XRF1-VHBR-TFN. In current industry trends it can be observed that the UHBR engine nacelle length-to-diameter ratios tend to be smaller to limit additional weight and drag [8]. Therefore it was decided to keep the overall engine length constant while increasing the BPR.

3.2. Nacelle and Core Shaping

The contours of the UHBR TFN are shown in Fig. 1. It comprises an outer nacelle and a core body with a plug. The plug is mounted to the core body by an inner pylon featuring a symmetric airfoil shape.

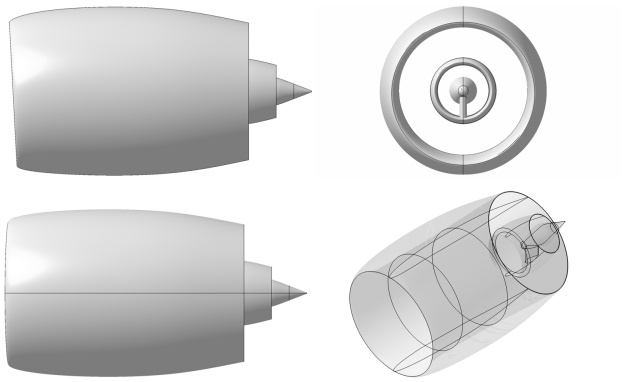

FIG 1. Isolated TFN design.

The shaping of the outer nacelle was aimed at reducing the shocks on the outer nacelle surface and thus wave drag. Figure 2 shows a Mach 1 iso-surface for the design with remains of a double shock system visible on the lower part of the nacelle. The inlet of the nacelle has a droop of 3° to account for the circulation of the wing. In order to get additional flow acceleration at the exhaust area the nozzle diameter was chosen to be slightly smaller than the highlight diameter.
The core body and plug were designed with two ideas in mind. First the streamtube contraction and therefore the position of the stagnation line on the inlet lip had to be controlled. This was achieved by sizing the core and plug accordingly to achieve a specified massflow. The core body diameter was used to approximately set the desired massflow and the plug size and horizontal position were then used to fine-tune the streamtube contraction ratio. Since no pylon was present in these isolated nacelle studies an

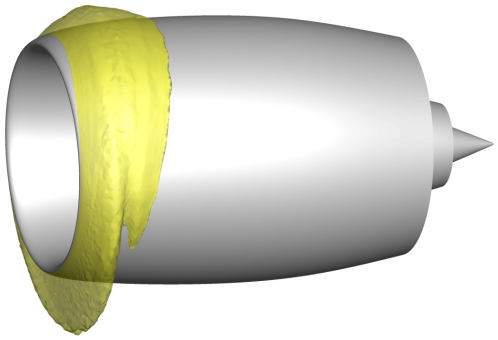

FIG 2. Isosurface of M=1 on outer nacelle contour.

additional geometric blockage of 5% was taken into account when computing the streamtube contraction ratio. A streamtube contraction of ε_F = 0.88 was targeted for this UHBR nacelle. The second idea concerning the core and plug assembly was that the proportions at the exhaust area look representative for typical high-bypass turbofan engines. This configuration was also beneficial for the buffet investigations due to additional flow displacement introduced on the wing lower side by the core and plug.

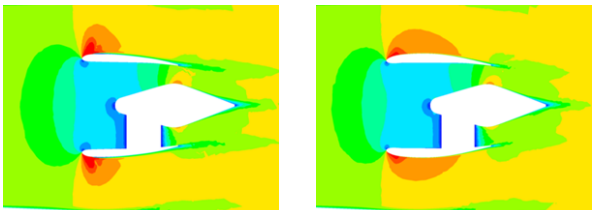

FIG 3. Elimination of shock induced separation on outer core surface. Contours of Mach number are shown.

Due to the plug inside the core body the stagnation line at the core lip was pushed inside the core inlet during early design iterations. This resulted in a strong flow acceleration around the core lip leading to shock induced separations which can be observed in the left part of Fig. 3. These flow separations were undesired on the core and the design was adapted to reduce the acceleration around the core lip as visible on the right in Fig. 3. The plug support pylon was already included in these isolated nacelle studies. It is a symmetric shape constructed from B-splines similar to an airfoil with increased thickness to account for structural constraints in advance.

4. INTEGRATION TO THE XRF1 WIND TUNNEL MODEL

Following the design of the isolated TFN the model was integrated to the XRF1 geometry. As a starting point for the integration studies the position of the existing VHBR nacelle was chosen. This allowed for the set up of a parametric CAD model of the pylon to be used in parameter studies on pylon shape and TFN position. Various parameters were varied of which only an excerpt is shown in this paper.
In the following some of the spanwise sections containing the main pressure measurement sections on the XRF1 wind tunnel model are used to show distinct features of the flow. Figure 4 gives an overview of the positions of the used sections.

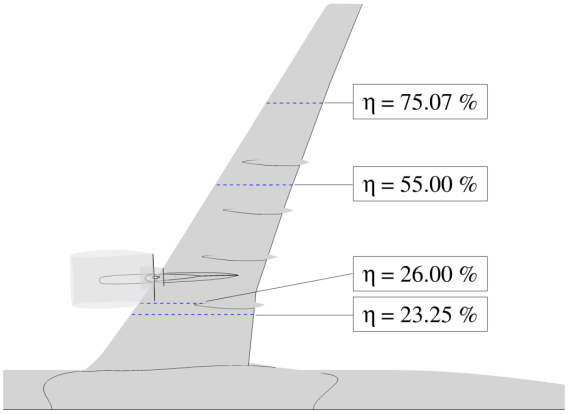

FIG 4. Selection of XRF1 wind tunnel model pressure sections.

4.1. Pylon design features

The target of the pylon design was to develope a pylon shape that is representative for typical turbofan engine mountings performing well under cruise conditions. Additionally, the pylon geometry was modified to help triggering the buffet phenomena on the wing lower side.
The spanwise position of the pylon wing intersection was constrained due to the position of the mounting holes for the pylon on the XRF1 wind tunnel model as depicted in Fig. 5.

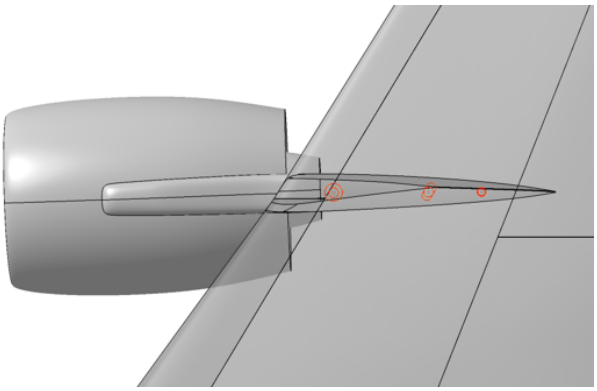

FIG 5. Top view of pylon geometry.

The pylon is asymmetric and twisted. This is a result of a relatively large toe-in angle of the nacelle that was required to align the nacelle inlet with the local flow under cruise conditions. It was observed that a large UHBR nacelle is more strongly influenced by the local flow displacement due to the fuselage. While the intersection of the pylon and the wing had to be aligned with the mounting hole positions the bottom of the pylon extending from the core body was aligned with the

nacelle axis resulting in a twisted shape. The pylon bottom surface was connected to the core inner surface with continuous curvature to allow for an undisturbed flow through the core body exhaust.
The rear extension of the pylon under the wing needed to fulfill multiple requirements. Firstly the existing mounting holes in the XRF1 wind tunnel model wing needed to be used which defined the pylon minimum length. Additionally the pylon should be as short as possible to minimize the wetted surface area and therefore skin friction drag. The pylon leading edge in the nacelle bypass was extended to the front to support the core and plug parts (see Fig. 6). An additional sweep was introduced to reduce the strong acceleration and resulting shock in the nozzle exhaust area around the pylon.

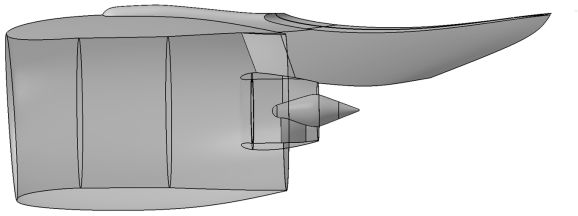

FIG 6. Side view of pylon geometry.

The pylon thickness increases from bottom to top towards the wing. This is beneficial for the applications in this project in multiple ways. Additional displacement under the wing behind the nacelle is introduced which helps triggering the transonic phenomena to be investigated. Additionally a thicker pylon is advantageous for placement and routing of instrumentation on the wind tunnel model.
The pylon leading edge on the nacelle, especially the crest line, was designed with the target to obtain a realistic shape from a structural point of view. Additionally the pylon nose shape as visible in Fig. 7 was adapted. The initial design included a round circular-arc like shape of the pylon nose cross section. This was deemed unrealistic and not suited for the buffet investigations. The more rectangular shape of the pylon nose, especially towards the wing intersection, introduces additional flow acceleration due to the stronger curvature. This results in a weakening of the boundary layer on the pylon making it more susceptible to shock induced separations.

4.2. Angle of attack variation

To get a better understanding of the sensitivities of the XRF1 with the integrated UHBR TFN, different angles of attack were investigated. The aim of this study was to find flow conditions that might be suitable to show the desired buffet effects in the inboard region. The investigations were carried out for a Mach number of 0.89 at a Reynolds number of 25 million. The results of the study are shown in Fig. 8. No transonic phenomena on the inboard wing lower side (η=23.25%) were observed for the angles of attack larger than 3°.

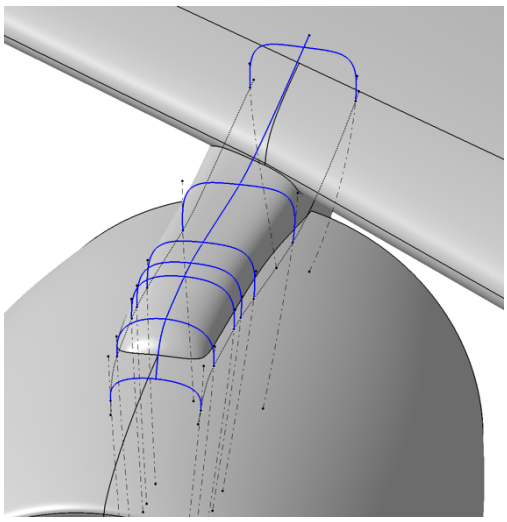

FIG 7. Pylon nose with cross-sections used for design.

However, if the angle of attack is reduced below 3°, accelerating flow can be observed in this area. For an angle of attack of 0° this results in a strong double shock under the wing at approximately 30-40% chord. The upper wing surface shows the expected behaviour of reduced pressure levels and upstream shock movement with decreasing angle of attack. For the 55% span wing section shocks at the wing lower were observed for angles of attack of 0° and 1°. The readers should note that the pressure distributions of the upper and lower side of the wing at α=0° and α=1° cross at 45% and 35% chord respectively. In front of the crossing point, the pressure on the wing lower side is therefore lower than on the wing upper side. As a result the suction peak is also located on the lower side of the wing. The flow on the upper wing surface shows reduced pressure levels and upstream shock movement with decreasing angle of attack again. At the outboard wing section the cross-over between the upper and lower surface pressure distributions is even more prominent for an angle of attack of 0° and 1°. The suction peaks are much stronger and shocks are formed on the wind lower side. It is noted that for the outboard wing section the crossover between the pressure distributions of the wing upper and lower side already occurs for an angle of attack of 2°.

4.3. Mach number variation

Following the angle of attack study a Mach number variation was conducted focusing on the development of the shock on the inboard wing lower side. Figure 9 shows three sectional pressure distributions for the wing at α=0°. The shock strength increases with increasing mach number and the shock position moves further downstream. At the inboard wing section the increase in shock strength is most pronounced when the Mach number is increased from 0.83 to 0.85. When the Mach number is further increased to 0.89 a double shock system develops which is comparable in shock strength to the shock observed for M=0.85.

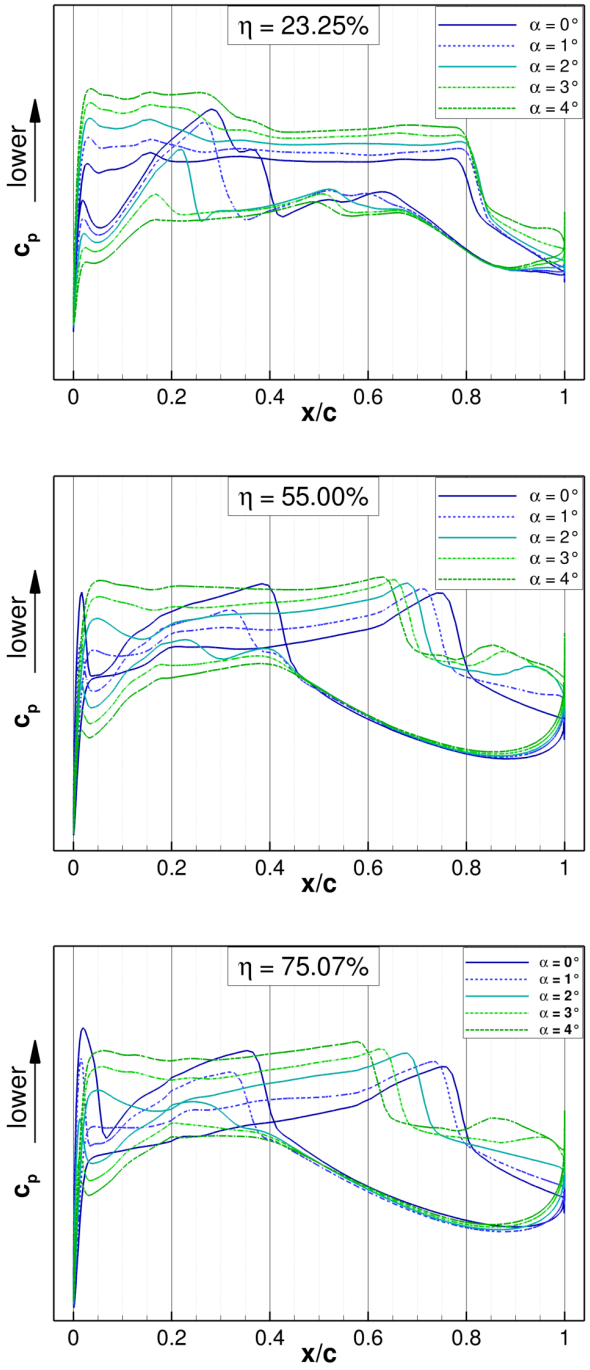

FIG 8. Influence of angle of attack on wing pressure distribution with installed UHBR TFN for M=0.89.

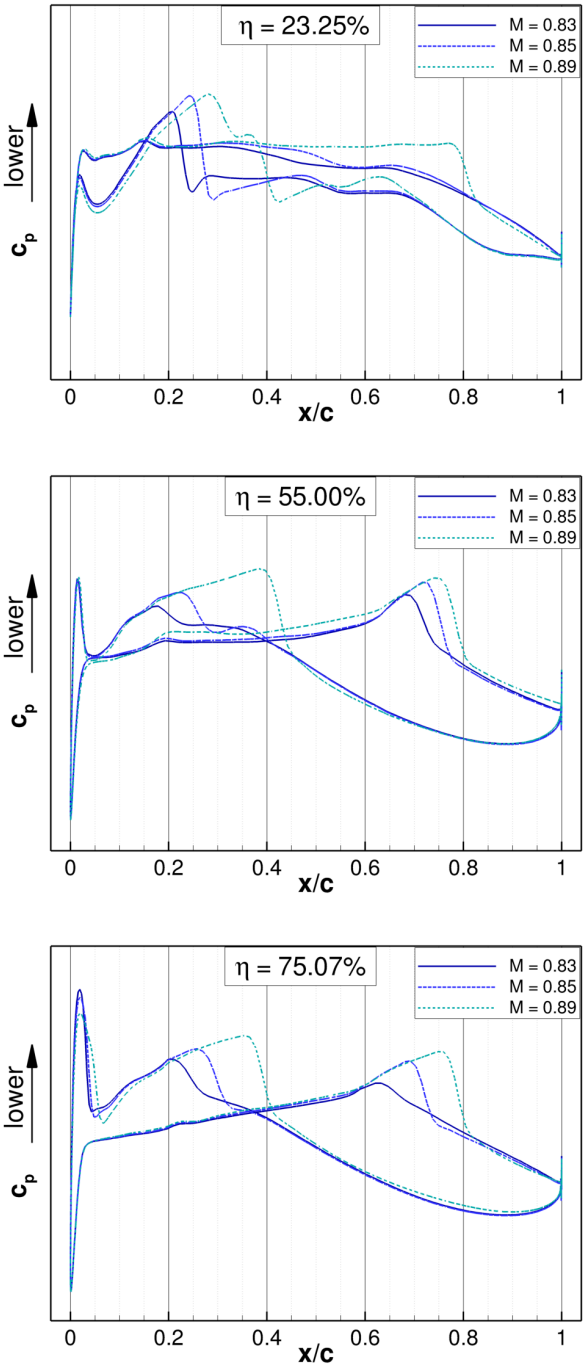

FIG 9. Influence of Mach number on wing pressure distribution with installed UHBR TFN for α=0°.

The origin of this double shock system for a Mach number of 0.89 is shown in Fig. 10. The spanwise position of η=23.25% is marked with a black line inboard of the UHBR nacelle. It is visible that two shock fronts cross this spanwise position. The upstream shock emanates from the UHBR nacelle trailing edge interacting with the wing pressure field. The second shock originates from the pylon. The interaction of these two shocks weakens the overall shock strength at the evaluation position of the pressure distribution at 23.25% span. This limits the possibility to increase the shock strength purely via the Mach number to trigger buffet phenomena. For the outboard wing sections no such integration effect is visible. As the Mach number increases shock strength increases and the shock position moves downstream almost linearly.

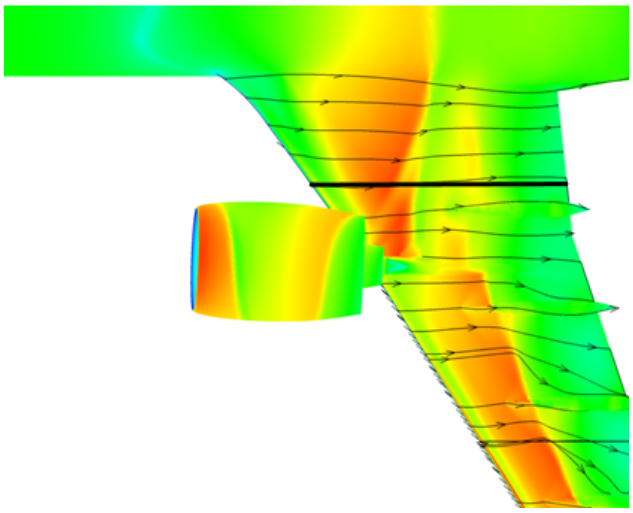

FIG 10. Pressure contour on wing lower side. M=0.89, α=0°

4.4. Geometric modifications

As an example of two geometric parameters investigated the influence of increased pylon thickness and increased nacelle overlap are shown as they had the strongest impact on the configuration. Increasing the pylon thickness was beneficial in both flow displacement leading to stronger transonic phenomena and installation space inside the pylon required for instrumentation on the wind tunnel model. Figure 11 shows pressure and skin friction coefficients for the 26% span position just inboard of the pylon (see Fig. 4) for a reference and a pylon with increased thickness as well as for a configuration with increased nacelle horizontal overlap. Due to the increased acceleration induced by the thicker pylon a stronger shock system forms further weakening the boundary layer flow. Additionally a small region of separated flow can be observed by negative $c_{f,x}$ values at 38% chord. The increased pylon thickness also results in an increase of the pylon width on the upper side leading edge. Nevertheless the flow around the pylon leading edge on the upper side is not much influenced by the increase in thickness.

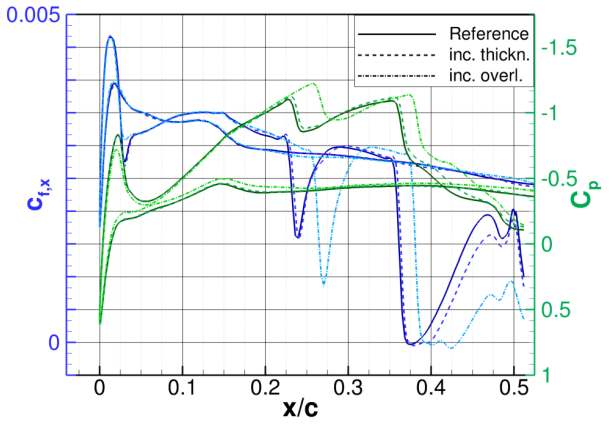

FIG 11. Influence of pylon thickness and nacelle overlap on pressure and skin friction coefficient for η=26% section. M=0.89, α=-2°

In addition the relative positioning of the wing nacelle assembly was varied. It is known that a larger horizontal overlap of nacelle and wing results in stronger aerodynamic interference effects due to the closer coupling [3]. The buffet effects to be investigated probably could have been triggered by selecting a very large horizontal overlap. Nevertheless an overlap this large would be unrealistic for a modern commercial transport aircraft and was considered not suitable for this project. Therefore the increase in actual overlap of nacelle and wing was investigated after having explored the potential of modifying the pylon to support the cause.
Different wing-engine couplings were investigated throughout these studies. It is know from literature that the effects of horizontal position variation of the engine are much more pronounced than the effects originating from variation of the vertical position [3]. Here the effect of an increase in actual overlap between nacelle and wing is shown. For this two horizontal positions were investigated. For the 0mm overlap (Reference) the nacelle trailing edge at its 12 o'clock position is located at the axial position of the wing leading edge. The 200mm overlap (inc. overl.) position of the nacelle is located 200mm to the rear. The impact on the shock induced separation on the wing lower side is depicted in Fig. 11. An increase in the spatial expansion of the separated area can be observed from the course of the $c_{f,x}$ plot around 40% chord. Due to the overlap the shock on the inboard wing lower side moves further downstream increasing in strength. This results in a heavier loading of the boundary layer which then is more prone to separation. For the shock front outboard of the pylon no such effect was observed.

5. PERFORMANCE EVALUATION

The final design of the integrated UHBR through flow nacelle was evaluated for different flow conditions performing TAU RANS simulations with the SSG/LRR-

lnω reynolds stress model [7]. It is known that a RANS RSM approach is not suitable to resolve buffet and detailed shock boundary layer interaction but it was deemed sufficient to get an estimate of the average flow phenomena. The assumption is made that strong shock induced separations observed in RANS RSM results indicate the existence of buffet phenomena in these regions.

5.1. Performance at lower wing buffet conditions

A Mach number of 0.84 and an angle of attack of -4° were defined as the reference flow conditions for lower wing buffet investigations. In the following the results obtained for the final configuration at these conditions are presented. An overview of the wing pressure distribution is given in Fig. 12 for the upper and lower side of the configuration.

Due to the negative angle of attack the pressure distribution on the wing upper side is very smooth with only moderate shocks and no observable flow separations. This is also supported by the skin friction lines plotted in Fig. 12. It should be noted here that the pressure distributions have to be interpreted with the negative angle of attack in mind. The wing lower surface is the suction side and the wing upper surface is the pressure side where the stagnation point is located.

The flow field on the wing lower side is of a very chaotic nature. Inboard of the UHBR nacelle a strong shock induced separation is visible from the skin friction lines and the contour of pressure coefficient. The extent of the shock induced flow separation can be seen from the recirculation region indicated by the surface streamlines in Fig. 12. The separated region extends from the axial position of the nacelle trailing edge up to the wing trailing edge and interferes with the flap track fairing. The flap track fairing thereby displaces the flow and forces the separated region towards the inboard direction. Flow separations were observed for the outboard wing lower side, nevertheless this will not be discussed any further in this paper since the focus lies on inboard effects induced by the nacelle installation and outboard flow separations were observed for the clean wing under these flow conditions as well.

A detailed look on the shock triggering the inboard flow separation is shown in Fig. 13. The isentropic Mach number is shown as contour variable and separated regions are indicated by solid and dashed lines. As can be seen the flow strongly accelerates in the junction formed by the wing, pylon and nacelle outer surface resulting in a shock on the wing lower surface and pylon slightly downstream of the nacelle trailing edge. This shock stretches inboard over half a nacelle diameter on the wing lower surface and is followed by a region of separated flow. On the pylon the flow coming out of the junction interacts with the bypass nozzle flow resulting in a shock accompanied by a flow separation at half pylon height at the axial position of the core trailing edge. On the nacelle outer surface itself

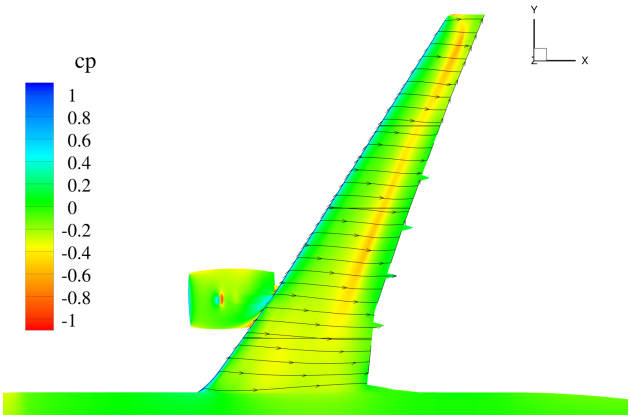

(a) Top view

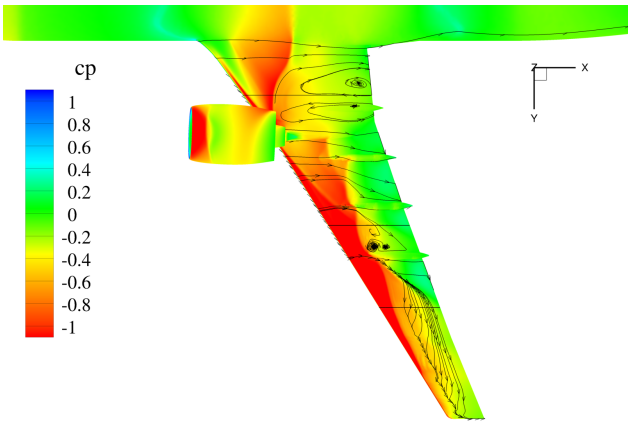

(b) Bottom view

FIG 12. Surface pressure distributions and streamlines for lower wing buffet conditions.

a shock induced separation is visible in the proximity of the trailing edge.

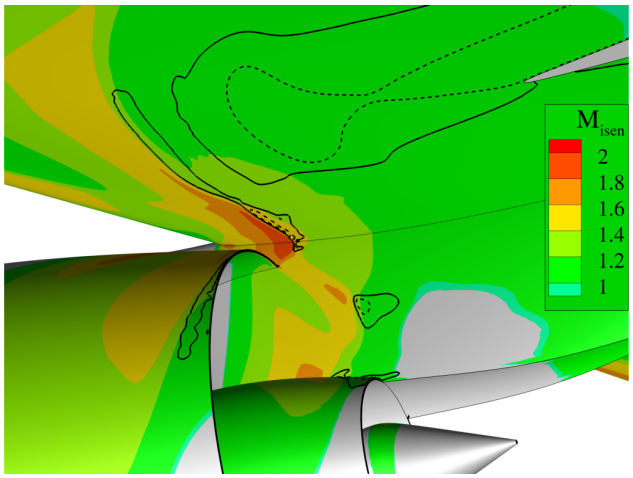

FIG 13. Visualisation of shock shock induced separation on wing lower side. Solid line indicate $c_{f,x} = 0$, dashed lines indicate $c_{f,x} < 0$.

The nacelle flow is characterized by the evaluation of pressure distributions at different circumferential positions in Fig. 14. The 20° and 79° sections are thereby oriented towards the inboard side while the 180° marks the 6 o'clock position. For orientation it should be mentioned that positive pressure coefficients are mostly seen for the interior part while the negative pressure coefficients correspond to the nacelle outer surface. The 20° circumferential position shows a stagnation point at the inlet followed by a slight acceleration around the inlet lip. For the most part of the nacelle length the pressure remains almost constant until the pressure field of the wing starts to interact with the nacelle. Following a slight increase in pressure up to 80% nacelle length the pressure drops significantly towards the trailing edge due to the flow accelerating in the narrowing channel formed by the nacelle, pylon and wing as visualized in Fig. 13. The pressure drop for the inner part of the nacelle towards the rear is explained by the vicinity of the pylon leading edge placed in the bypass.
A similar behavior can be observed for the pressure distribution at the 79° position on the forward half of the nacelle.The pressure drop at the outer part of the nacelle due to the interference with the wing starts at around 50% nacelle length and results in a shock at 95% length. This shock triggers a flow separation that was already visible in Fig. 13. The pressure drop towards the rear at the inner surface is significantly lower compared to the 20° section but still observable. For the bottom nacelle section at 180° circumferential position a strong suction peak develops on the outside inlet lip. At 17% nacelle length a shock occurs resulting in a small shock induced separation. At the rear part of the nacelle the flow accelerates again slightly due to surface curvature before returning to equilibrium towards the trailing edge.

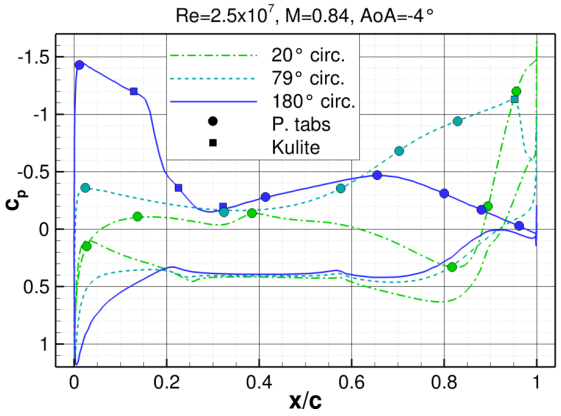

FIG 14. Nacelle pressure distributions and instrumentation.

5.2. Performance at cruise conditions

After having defined the final design geometry of nacelle and pylon the configuration was simulated for cruise conditions to ensure that the engine integration does not have any severe detrimental effects on cruise performance, e.g. flow separations on the wing upper side or any vortices disturbing the pressure distribution on the wing. Neither the surface pressure distribution nor the flow field show any indications that strong adverse installation effects are present under cruise conditions. Nevertheless, the design still offers potential for improvement in terms of efficiency at the cruise point.

6. INSTRUMENTATION

The wind tunnel model of the through flow nacelle designed in this work was equipped with instrumentation to allow a detailed analysis of the surrounding flow during and after the experiments. A total of 14 Kulite unsteady pressure sensors and 18 pressure taps were installed on the model of the UHBR through flow nacelle.
The pylon is equipped with a total of 10 unsteady pressure sensors from Kulite which are all located at the inboard side of the pylon. The Kulites are arranged in two rows as depicted with black squares in Fig. 15. An upper row of 6 Kulite sensors is located in the proximity of the pylon wing intersection and a lower row of 4 Kulites is placed at around half pylon height. In Fig. 15 contours of isentropic Mach number for lower wing buffet conditions are shown to explain the reasoning behind the Kulite placement. Both rows of Kulites are arranged such that they are able to capture any shock movement occurring in the pylon wing intersection or on the pylon due to buffet. The axial extent of the Kulite placement is thereby chosen to allow measurements for multiple operating points for lower wing buffet investigations. One pressure tap is located on the pylon as a reference for the interior bypass flow. It is located at the inboard side of the pylon leading edge inside the bypass nozzle.

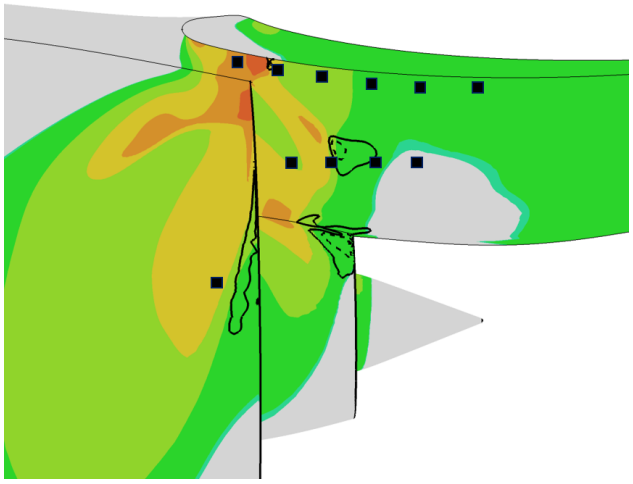

FIG 15. Kulite installation on pylon and nacelle. Contour colours depict isentropic Mach number. Solid lines indicate flow separations.

The nacelle is equipped with a total of 4 unsteady pressure sensors and 17 pressure taps arranged in three circumferential sections. The sections are located on circumferential positions of 20°, 79° and 180° respectively. In Fig. 16 pressure contours are shown for the nacelle as viewed from the inboard side. The 20° and 79° sections are marked by blue lines with the positions of the sensors marked by black symbols. Figure 17 shows the nacelle as viewed from the bottom accorcdingly with the 180° section marked by a blue line. Pressure taps are displayed by circles and Kulites are represented by squares.

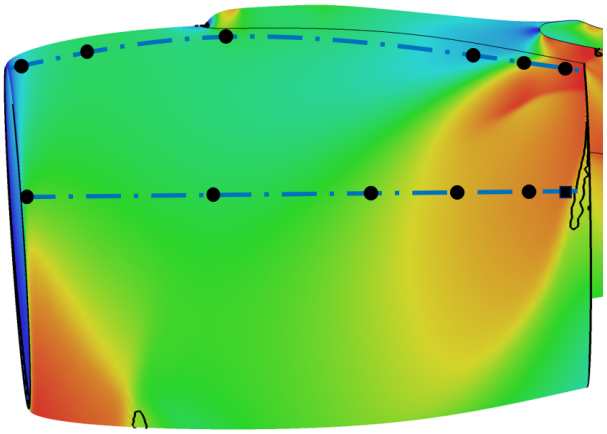

FIG 16. Nacelle pressure contour and measurement sections as viewed from the inboard side.

All Kulites are placed in regions were shock boundary layer interaction and shock induced flow separation is expected. For the 79° section the Kulite was placed as close to the nacelle trailing edge as design space allowed to capture the shock induced separation marked by the black curve in Fig. 16. The Kulites on the 180° section were placed around the shock

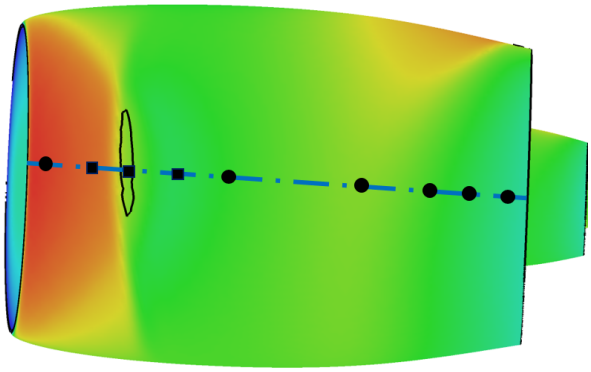

FIG 17. Nacelle pressure contour and measurement sections as viewed from the bottom.

induced separation region. The pressure taps were distributed between the three sections with the target to be able to reproduce the main shape of the pressure distributions during the wind tunnel investigations. The is distribution of the pressure tabs along the c_p distribution is also depicted in Fig.14.

7. CONCLUSION

In this work the design of a UHBR through flow nacelle to be used in conjunction with the XRF1 wind tunnel model was presented. The design target to develop a through flow nacelle representative of a modern UHBR turbofan engine that allows for investigation of buffet phenomena on the wing lower side under high-speed off-design conditions was reached. At the same time the nacelle exhibits reasonable performance in cruise keeping the link towards industrial applications. The through flow nacelle is equipped with a core body and a plug, giving the nozzle area a representative appearance. Additionally a pylon was constructed connecting the nacelle to the XRF1 wing. The assembly of through flow nacelle, pylon and XRF1 wing and fuselage shape was tested for design and off-design performance with the DLR TAU code. All design criteria were met, explicitly a strong shock induced separation was observed for off-design conditions allowing for investigation of buffet phenomena. No detrimental effects were observed for cruise conditions.

ACKNOWLEDGEMENT

The authors would like to thank the Helmholt Gemeinschaft HGF (Helmholtz Association) for funding this research and Airbus for providing the baseline wind tunnel model geometry. Moreover we gratefully acknowledge the Deutsche Forschungemeinschaft DFG (German Research Foundation) for providing the framework of this research given by the research unit FOR 2895.

Contact address:

sebastian.spinner@dlr.de

References

[1] D. L. Daggett, S. T. Brown, and R. T. Kawai. Ultra-efficient engine diameter study. Technical Report CR-2003-212309, NASA, 2003.

[2] H. Hoheisel. Aerodynamic aspects of engine-airframe integration of transport aircraft. *Aerospace Science and Technology*, (7):475–487, 1997.

[3] R. Rudnik, C.-C. Rossow, and H. Frhr. v. Geyr. Numerical simulation of engine/airframe integration for high-bypass engines. *Aerospace Science and Technology*, 6, 2002.

[4] Thomas Gerhold. Overview of the hybrid rans code tau. In Norbert Kroll and Jens K. Fassbender, editors, *MEGAFLOW - Numerical Flow Simulation for Aircraft Design*, pages 81–92, Berlin, Heidelberg, 2005. Springer Berlin Heidelberg.

[5] S.R. Allmaras, F.T. Johnson, and P.R. Spalart. Modifications and clarifications for the implementation of the spalart-allmaras turbulence model. In *7th Internation Conference on Computational Fluid Dynamics*, Big Island, Hawaii, 2012.

[6] M.L. Shur, M.K. Strelets, A.K. Travin, and P.R. Spalart. Turbulence modeling in rotating and curved channels: Assessing the spalart-shur correction. *AIAA Journal*, 38(5):784–702, 2000.

[7] R. Cecora, R.-D. Radespiel, , B. Eisfeld, and A. Probst. Differential reynolds-stress modeling for aeronautics. *AIAA Journal*, 53(3):739–755, 2015.

[8] A. Magrini, E. Benini, H.-D. Yao, J. Postma, and C. Sheaf. A review of installation effects of ultra-high bypass ratio engines. *Progress in Aerospace Sciences*, (119), 2020.